51-nm Uniform-Intensity Tuning of Superstructure Grating Active-DBR Laser for 2-μm Wavelength Band

Takahiko Shindo, *Member, IEEE*, Yuta Ueda, *Member, IEEE*, Makoto Shimokozono, Tomonari Sato, Wataru Kobayashi, Shigeru Kanazawa, *Senior Member, IEEE*, Mingchen Chen, and Hideaki Matsuzaki, *Senior Member, IEEE*

***Abstract*—To suppress the fluctuation of light intensity during wavelength tuning caused by carrier induced optical loss, we utilized a single quantum well (SQW) inserted into the bulk core layer of distributed Bragg reflectors (DBRs), called an active DBR structure, for a 2-μm-wavelength superstructure grating (SSG-) DBR laser. In the active DBR structure, some injected currents in the DBR regions are consumed for an optical gain in the inserted SQW, which suppresses the optical loss in the bulk core layer induced by the free-carrier absorption. The SSG-DBR laser fabricated with the active DBR structure exhibited a more than 8-nm lasing wavelength shift of a single SSG-DBR reflection peak. In addition, the reduction of light intensity was less than 2.7 dB when the total injection current of the front and rear DBR regions was 200 mA. This is significantly smaller than that of a conventional SSG-DBR laser that has the same device structure except for the SQW in the DBR regions, although a relatively large current was required for the wavelength shift. Evaluations of the lasing characteristics under various combinations of the front and rear DBR currents demonstrated that all seven SSG-modes could be selectively oscillated for wavelength tuning. In addition, the measured fluctuation of light intensities was less than 5 dB for almost all conditions even when the front and rear DBR currents were individually changed from 0 up to 100 mA. Furthermore, the active-DBR type laser simultaneously attained the quasi-continuous tuning range of 51.2 nm and the fluctuation of light intensity across the whole range of less than 2.5 dB which represents a significant suppression compared to the conventional SSG-DBR laser with the same laser cavity design.**

***Index Terms*—Distributed Bragg reflector laser, semiconductor laser, tunable lasers.**

I. Introduction

TUNABLE diode laser-based gas spectroscopy is an attractive method for gas sensing because it enables us to reasonably construct a measurement system with high-speed, high-sensitivity, and high-specificity characteristics. For CO_2 gas sensing, the wavelength range of around 2 μm is more useful than the 1.55-μm range that is commonly used for optical communication systems due to a relatively strong absorbance of CO_2 and a little interference from H_2O. Thus, wavelength tunable semiconductor laser diodes emitting around 2-μm wavelength are a key component to construct an effective CO_2 gas sensing system. For the light source beyond the 1.8-μm wavelength, GaSb-based lasers have a high-power operation advantage due to their relatively large material gain [1]–[4]. On the other hand, InP-based material systems are also attractive for light sources of this wavelength range because we can use mature fabrication processes originally developed for telecommunication devices that are now well-established. Various InP-based semiconductor lasers in this wavelength range have been demonstrated, such as Fabry-Pérot lasers [5], [6] and distributed feedback (DFB) lasers [7]–[9]. As a wavelength tunable light source for the 2-μm range, an InP-based monolithic integrated laser using voltage controlled Mach–Zehnder interferometers was demonstrated with a wide tuning range of over 30 nm [10]. Distributed Bragg reflector (DBR) lasers [11]–[13] can also achieve wide and fast wavelength tuning characteristics with a small footprint, because the lasing wavelength can be electrically tuned due to a refractive index change induced by injected carriers [14]. We previously demonstrated a 2-μm-wavelength InGaAs DBR laser with the wide tuning range of over 10 nm [15]. In addition, a practical CO_2 detection has been demonstrated using this laser [16]. We have also utilized a superstructure grating (SSG) [17]–[21], which is a special grating structure with multiple reflection peak characteristics [22], [23], for the 2-μm-wavelength DBR laser to further increase the tuning range, and demonstrated the wide tuning range of over 50 nm [24]. Although a longitudinal mode hop is inherently unavoidable for SSG-DBR lasers, the lasing wavelength can be accurately tuned at any value in the whole tuning range. Therefore, the lasers can achieve quasi-continuous wavelength sweeping by step tuning with constant frequency spacing, which enables wide and fast scanning of the absorption lines of target gasses [25], [26]. One of the remaining issues in the 2-μm-wavelength SSG-DBR laser is the large fluctuation of light

Manuscript received February 18, 2022; revised April 6, 2022; accepted April 29, 2022. Date of publication May 9, 2022; date of current version May 19, 2022. *(Corresponding author: Takahiko Shindo.)*

Takahiko Shindo, Yuta Ueda, Shigeru Kanazawa, and Mingchen Chen are with the NTT Device Innovation Center, NTT Corporation, Atsugi-shi 243-0198, Japan (e-mail: takahiko.shindo.xu@hco.ntt.co.jp; yuta.ueda.dh@hco.ntt.co.jp; shigeru.kanazawa.vn@hco.ntt.co.jp; mingchen.chen.gn@hco.ntt.co.jp).

Makoto Shimokozono, Tomonari Sato, Wataru Kobayashi, and Hideaki Matsuzaki are with the NTT Device Technology Labs, NTT Corporation, Atugi-shi 243-0198, Japan (e-mail: makoto.shimokozono.cu@hco.ntt.co.jp; tomonari.sato.gn@hco.ntt.co.jp; wataru.kobayashi.xw@hco.ntt.co.jp; hideaki.matsuzaki@lumentum.com).

Digital Object Identifier 10.1109/JPHOT.2022.3172695

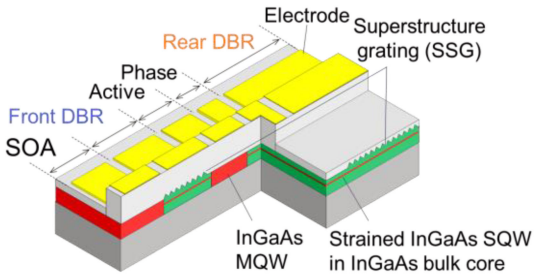

Fig. 1. Schematic structure of 2 μm wavelength SSG-DBR laser.

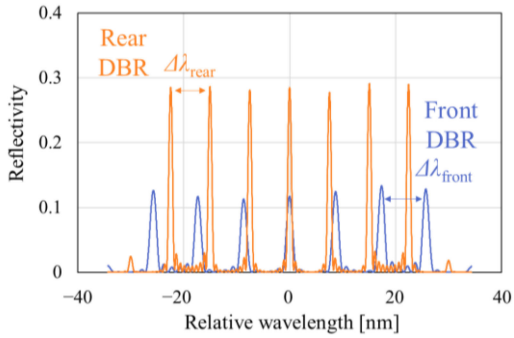

Fig. 2. Calculated reflection spectra of front and rear SSG-DBRs.

intensity during wavelength tuning, which stems from the optical loss in the DBR regions due to free-carrier absorption induced by the injected current. For the 1.55-μm-wavelength tunable laser utilizing carrier-plasma effect, the integrated semiconductor optical amplifier (SOA) has generally been used to equalize the light intensity during wavelength tuning [25]–[28]. However, the fluctuation of the intensity is more significant for the 2-μm wavelength, because the free-carrier absorption becomes larger as the wavelength lengthens [14]. When the fluctuation reaches the dB level, it would be difficult to completely equalize it by changing the SOA current. As a fundamental solution, we developed a 2-μm-wavelength DBR laser with a single quantum well (SQW) inserted into the bulk core layer [29], which we called an active DBR structure [30], [31]. In this structure, the parts of injection currents in the DBR regions for wavelength tuning are consumed for an optical gain in the SQW to compensate the optical loss due to the free-carrier absorption in the bulk core layer in the DBR regions.

In the current work, we have newly designed and demonstrated a 2-μm-wavelength SSG-DBR laser with the active DBR structure [32] to improve the uniformity of light intensity during wavelength tuning. To clarify the effect of the active DBR structure, we also fabricated a conventional SSG-DBR laser with the same structure except for the SQW in the tuning regions. The basic lasing characteristics of the fabricated active-DBR laser were evaluated and compared with those of the conventional device. We found that the threshold current and light intensity were the same level for both the proposed and conventional lasers. In addition, the reduction of light intensity was dramatically suppressed thanks to the optical gain in the SQW, although relatively large currents were required for wavelength tuning. Furthermore, we demonstrated that the fabricated device attained the quasi-continuous tuning range of over 50 nm and exhibited a significantly small fluctuation of light intensity (less than 2.5 dB) across the whole tuning range.

II. Basic Device Structure and Concept of Active DBR

Fig. 1 shows the schematic structure of the SSG-DBR laser. The laser cavity formed on an InP substrate consists an active region, a phase control (PC) region, and front/rear DBR regions. A semiconductor optical amplifier (SOA), which has the same multi-quantum-wells (MQWs) as the active region, is also formed on the front of the laser cavity. These multiple components are monolithically integrated on the same chip by using a dry etching and regrowth process called a butt-joint technique. The length of the active region and the SOA are 350 and 430 μm, respectively. The lengths of the front/rear DBR regions and PC region are 440/830 and 100 μm, respectively. We designed the superstructure gratings (SSGs) with the coupling coefficient of 40 cm^{-1} for the 2-μm-wavelength range and formed them on the DBR regions by electron beam lithography. The SSGs have multiple periodic reflection peak characteristics due to the multiple phase shifts formed in the SSGs. We optimized the SSGs to have uniform reflectivity between each reflection peak. The details of the design method for the SSGs with multiple phase shifts are provided in prior work [17], [20]. The calculated reflection spectra for the front and rear SSG-DBRs are shown in Fig. 2, where both the front and rear SSG-DBRs are designed to have seven-reflection peaks. As we can see, all reflection peaks for both the front and rear SSGs have almost uniform reflectivity. In addition, there is a slight difference in the reflection peak spacing between the front ($\Delta\lambda_{\mathrm{front}}$) and rear ($\Delta\lambda_{\mathrm{rear}}$) SSG-DBRs so that the Vernier effect can be used. The two SSGs are thus able to operate as wavelength-selective reflectors because only one combination of reflection peaks coincides at any time. The lasing wavelength can be flexibly selected by changing the combination of reflection peaks of the front and rear SSG-DBRs. In addition, both $\Delta\lambda_{\mathrm{front}}$ and $\Delta\lambda_{\mathrm{rear}}$ are designed to be smaller than the amount of wavelength shift for a single reflection peak so as to achieve a quasi-continuous tuning. Otherwise, wavelength gaps in which the lasing wavelength cannot be tuned would occur between each reflection peak.

Fig. 3 shows cross-sectional views of a) the active region/SOA, b) the DBR region for the conventional device, and c) the DBR region for the active-DBR laser. For the active region and SOA, a strained InGaAs/InGaAs MQW was sandwiched between the lattice-matched InGaAs layers, which are lattice-matched to InP and have the bandgap wavelength of 1.7 μm. InGaAsP separate confinement heterostructure (SCH) layers with the bandgap wavelength λ_{bg} of 1.3 μm were also inserted into the upper and lower boundaries between the InGaAs core layer and InP cladding layers. The InGaAs/InGaAs MQWs consist of 10-nm-thick quantum wells with 1.7% compressive strain and 13-nm-thick barrier layers with 1% tensile strain. The

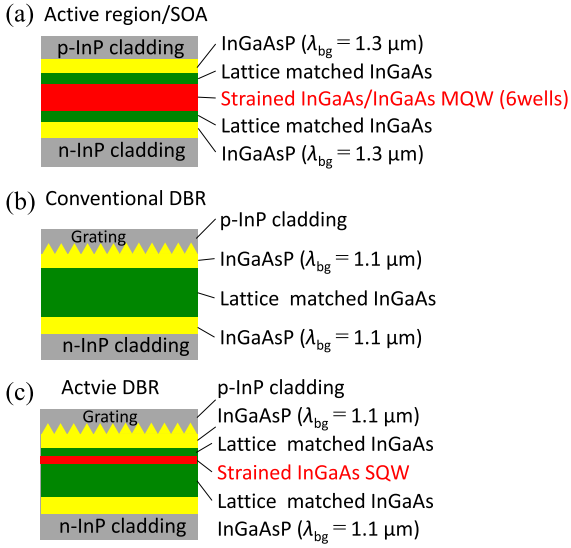

Fig. 3. Cross-sectional structure of (a) active region and SOA, (b) conventional DBR, and (c) active DBR structure.

number of quantum wells was designed to be six. The measured peak wavelength of the photoluminescence (PL) spectrum for the InGaAs/InGaAs MQW was 2015 nm. The conventional DBR structure was based on the InGaAs bulk core layer, and InGaAsP layers with the λ_{bg} of 1.1 μm was used for the SCH layers. The superstructure grating was formed on the boundary between the upper InGaAsP SCH and p-doped cladding layer as shown in Fig. 3(b). The phase control (PC) region also has the same cross-sectional structure as the DBR regions except that no grating was formed. The active DBR structure is also based on a lattice-matched InGaAs core layer with an InGaAsP SCH layer ($\lambda_{\mathrm{bg}} = 1.1$ μm), as shown in Fig. 3(c). In addition, for the active DBR, a compressively strained InGaAs single quantum well (SQW), which has the same material composition as the MQW for the active region and SOA, was inserted into the lattice-matched InGaAs bulk core layer. Therefore, the PL wavelength for the SQW was also 2015 nm. The position of the SQW was determined by considering the optical confinement factor in the well that affects the balance between optical gain and wavelength tuning [29]. The total thickness of the core layer including the SQW was 300 nm which is the same as that for the conventional DBR structure shown in Fig. 3(b). To clarify the effect of the SQW in the active DBR structure, we also fabricated a conventional SSG-DBR laser using the same fabrication process. The conventional device has the same cavity design as the active-DBR laser, and the only difference between the two is the presence or absence of the SQW in the core layer of the DBRs and PC region.

Fig. 4 shows the schematic band structure of (a) the conventional and (b) the active DBR structures. The refractive index change Δn due to the carrier-plasma effect is explained as [14]

$$\Delta n = -\frac{e^2\lambda^2}{8\pi^2 c^2 \varepsilon_0 n}\left(\frac{\Delta N}{m_e} + \frac{\Delta P}{m_h}\right) \quad (1)$$

where n is the refractive index of the bulk core layer, and ΔN and ΔP, m_{e} and m_{h} are the densities and effective masses for

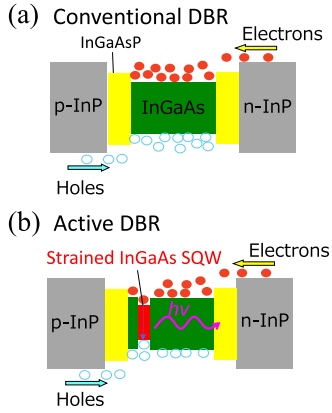

Fig. 4. Schematic band structure of (a) conventional DBR and (b) active DBR structure.

electrons and holes, respectively. The other symbols have the usual meanings. In the conventional DBR, the refractive index of the InGaAs bulk core layer becomes smaller as the carrier densities ΔN and ΔP in the InGaAs core layer increase due to the injected current. As a result, the reflection peak of the DBR region shifts to a shorter wavelength, and the optical loss due to free-carrier absorption also increases in the InGaAs bulk core layer. For the 2-μm wavelength, the optical loss due to free-carrier absorption is significantly larger than that for the 1.55-μm wavelength range because the free-carrier absorption has a dependence on the squared wavelength λ^2. In contrast, in the active DBR structure, some parts of the electrons and holes are recombined in the SQW and consumed for an optical gain. In this way, the reduction of the light intensity can be suppressed, although the carrier densities ΔN and ΔP are relatively small compared with those for the conventional DBR, even under the same current condition. In our previous work, the efficiency of the wavelength shift for the active-DBR laser was explained with assumed rate equation in which the carrier consumption for an optical gain in the SQW is included, and compared with the efficiency of the conventional DBR laser [29]

III. Basic Performance of SSG-DBR Laser

A. Lasing Characteristics

We first measured the injection current for the active region versus light intensity (*I-L*) characteristics of the fabricated SSG-DBR lasers with the active DBR and conventional DBR. Fig. 5(a) shows the operation setup of the SSG-DBR lasers for this measurement. The driving temperature of the laser chips was set to 25°C. The SOA current (I_{SOA}) was fixed at 90 mA, and the current for the active region (I_{act}) was swept from 0 to 120 mA. In addition, the front/rear DBRs and the PC region were electrically connected and driven with the same current source as I_{tune} to mimic an actual driving condition with a simple configuration. Under this condition, the carrier densities in the front and rear DBR regions are always the same so that the same reflection peaks of the front and rear SSG-DBRs always coincide with each other. In this way, the cavity loss originating from the front and rear SSGs can be maintained for all I_{tune}

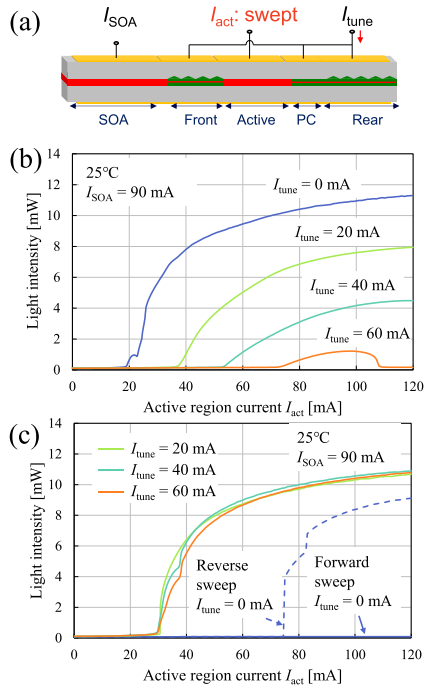

Fig. 5. (a) Operating setup of SSG-DBR laser. I-L characteristics for (b) conventional SSG-DBR laser and (c) SSG-DBR laser with active DBR structure.

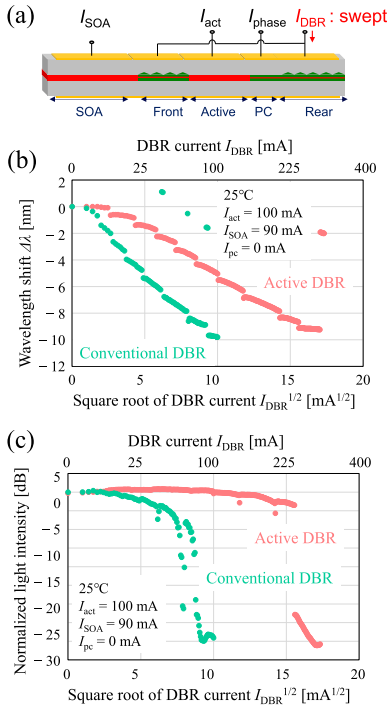

Fig. 6. (a) Operating setup of SSG-DBR laser. (b) Wavelength shift and (c) light intensity as dependence on the DBR current.

conditions. The measured *I-L* characteristics under various $I_{\rm tune}$ conditions for the conventional SSG-DBR laser are shown in Fig. 5(b). We can clearly see that the light intensity and threshold current were constantly degraded as the $I_{\rm tune}$ increased. This was because the injected carriers in the tuning regions induced a large optical loss caused by the free-carrier absorption. For the conventional SSG-DBR laser, this change of the internal loss caused a large fluctuation of the light intensity during wavelength tuning. The measured *I-L* characteristics of the fabricated SSG-DBR laser with the active DBR structure are shown in Fig. 5(c). In this device, no lasing oscillation was observed for the $I_{\rm tune}$ of 0 mA when the $I_{\rm act}$ was swept forward from 0 to 120 mA. This was caused by the large optical absorption loss in the SQW in the active DBRs and PC region under the $I_{\rm tune}$ of 0 mA. Lasing oscillations when the $I_{\rm tune}$ was over 20 mA were observed, as the optical loss in the SQW was compensated due to the injected $I_{\rm tune}$. In addition, lasing oscillation was observed and maintained even for the $I_{\rm tune}$ of 0 mA and the $I_{\rm act}$ of 120 mA, once the $I_{\rm tune}$ was changed to 20 mA, and then returned to 0 mA. The *I-L* curve for the $I_{\rm tune}$ of 0 mA with reverse sweep of the $I_{\rm act}$ is also plotted on the graph with a dashed line. In this case, the $I_{\rm act}$ was reversely swept from 120 mA to 0 mA after the laser was oscillated by changing the $I_{\rm tune}$. For the reverse sweep, the *I-L* curve nonlinearly jumped at the $I_{\rm act}$ of around 75 mA because of the saturable absorption effect of the active DBR structure. However, these results indicate that the lasing oscillation can be maintained during wavelength tuning even under small current conditions of tuning regions, once the lasing oscillation has occurred under a sufficiently large $I_{\rm act}$. The threshold current and light intensity were almost the same level when the $I_{\rm tune}$ was changed from 20 to 60 mA. Therefore, under these conditions, the optical loss induced by the $I_{\rm tune}$ was almost perfectly compensated by the optical gain in the inserted SQW in the active DBR structure. This effect enables us to suppress the fluctuation of light intensity during wavelength tuning.

B. *Carrier-Induced Wavelength Shift and Optical Loss*

Next, we evaluated the lasing wavelength shift and light intensity as dependence on the DBR current for both devices. The operation set-up is shown in Fig. 6(a). The active region, SOA, and PC region were constantly driven by individual current sources. The $I_{\rm act}$, $I_{\rm SOA}$, and phase control current ($I_{\rm PC}$) were set to 100, 90, and 0 mA, respectively. The front and rear DBR regions were electrically connected and simultaneously swept ($I_{\rm DBR}$) by the same current source. Before sweeping, the laser was oscillated by changing the $I_{\rm DBR}$. Under this condition, the refractive index change due to the carrier-plasma effect in the front and rear DBRs is always the same, which means the same reflection peaks of the front and rear SSG-DBRs always coincide with each other. Therefore, the wavelength shift for a single reflection peak of SSGs caused by the reduction of the refractive index due to carrier-plasma effect can be evaluated. In addition, the cavity loss originating from the front and rear SSG-DBRs is always fixed for all current conditions. We measured the lasing wavelength and light intensity with a spectral analyzer and then normalized the results based on the values under the 0 mA $I_{\rm DBR}$ condition. Normalized wavelength shifts and light intensities for the conventional SSG-DBR laser and the active-DBR laser are plotted in Fig. 6(b) and (c), respectively, as dependence on the square root of the $I_{\rm DBR}$. As the $I_{\rm DBR}$ increased, the lasing wavelength became shorter due to the carrier-plasma effect.

Even when a relatively large current was injected into the DBR regions, the slope of the wavelength shift was almost constant. This indicates that the thermal effect caused by the injected current does not have a significant impact on the wavelength tuning, and the refractive index change due to carrier-plasma effect is dominant even for relatively large current conditions. The discontinuous point on the curve of the wavelength shift is caused by the longitudinal mode hop (Fabry-Pérot mode hop). For the conventional DBR, the light intensity rapidly decreased as the I_{DBR} increased. The I_{DBR} should be less than 50 mA so that the reduction of light intensity is less than 5 dB, and in this case, the wavelength shift was about 7.5 nm for the conventional device. In contrast, the wavelength shift for the active DBR laser was smaller, since part of the injected current in the DBR regions is used for optical amplification in the SQW and does not contribute to the wavelength shift. However, the decrease in light intensity was dramatically suppressed to about 2.7 dB even when the I_{DBR} increased to more than 200 mA. Under this condition, the wavelength shift of more than 8 nm was achieved. These results demonstrate that a small fluctuation of light intensity and a sufficient wavelength shift can be simultaneously achieved by using the active DBR structure.

For both devices, the wavelength shift in the small current region of less than about 2 $\mathrm{mA}^{1/2}$ was very small. This was probably due to the non-radiative surface recombination in the side wall of the ridge-mesa structure of the laser. In this current region, the injected carriers in the DBR regions are consumed to fill the non-radiative recombination center and do not contribute to the increase in the carrier density in the InGaAs core layer. Especially for the active-DBR laser, a relatively large current is required when the wavelength shift begins, probably due to the band-edge absorption in the SQW in addition to the surface recombination.

C. Wavelength Tuning Characteristics

Fig. 7 shows the basic wavelength tuning characteristics of the active-DBR laser compared with those of the conventional one. In this evaluation, the I_{act}, I_{SOA}, and I_{PC} were set to 100, 90, and 0 mA, respectively, and the front (I_{front}) and rear (I_{rear}) DBR currents were then individually swept. When one was swept, the other was set to 0 mA. The wavelength of the first lasing mode was measured by using a spectrum analyzer. In Fig. 7, the lasing wavelength dependence on the I_{front} and I_{rear} is plotted on the left and right sides of the graph, respectively. As we can see, the lasing mode hopped to the longer one when the I_{front} increased, while in contrast, it hopped to the shorter one when I_{rear} increased. In addition, the seven SSG-modes (1–7 in the graphs) were clearly observed. Each SSG-mode corresponds to a different combination of reflection peaks of the front and rear SSG-DBRs. For both devices, the wavelength difference between each SSG-mode was about 8 nm. As we can see in Fig. 6(a), the wavelength shift for a single reflection peak was more than 8 nm, which is larger than the SSG-mode spacing shown in Fig. 7, for both devices. This indicates that each SSG-mode can be shifted to overlap the wavelength of the next SSG-mode. Therefore, both the conventional and proposed

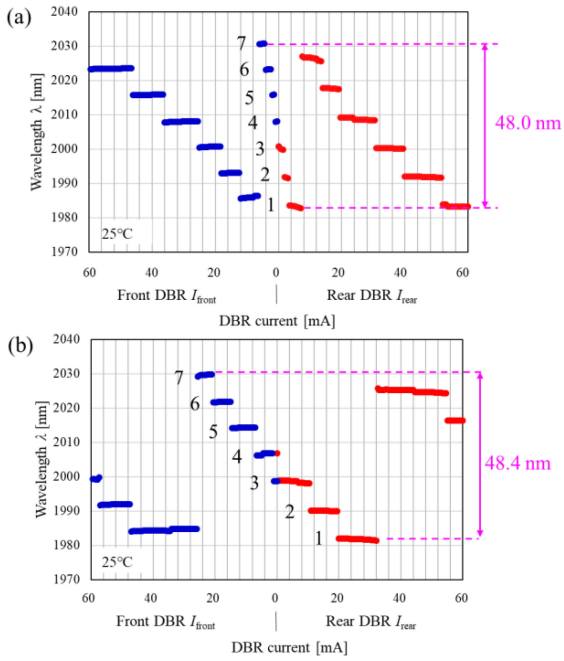

Fig. 7. Wavelength tuning characteristics for (a) conventional SSG-DBR laser and (b) SSG-DBR laser with active DBR.

lasers can cover the whole wavelength range without gaps by using all seven SSG-modes. For the conventional SSG-DBR laser, the lasing wavelength hopped to the next SSG-mode with a relatively small change of currents for the DBR regions. In contrast, a relatively large change of currents was required to change the oscillating SSG-mode for the SSG-DBR laser with the active DBR structure, as parts of the injected carriers were consumed for the optical amplification in the SQWs, and they did not contribute to changing the refractive index. However, all seven SSG-modes were visible, although relatively large currents were required. These findings demonstrate that all seven SSG-modes could be selectively used for wavelength tuning, and our new SSG-DBR laser with the active DBR structure was successfully fabricated.

D. Wavelength and Intensity Maps

Next, we evaluated the wavelength tuning characteristics of both devices under various conditions of DBR currents. In this measurement, the I_{front} and I_{rear} were independently changed in increments of 1.0 mA. The lasing wavelengths for all combinations of I_{front} and I_{rear} are plotted in Fig. 8. The I_{PC} was always set to 0 mA for both devices, and I_{act} and I_{SOA} were 100 and 90 mA, respectively. For the conventional SSG-DBR laser, the DBR currents were swept from 0 to 30 mA, as shown in Fig. 8(a). For the active-DBR laser, the maximum currents were set to 100 mA in order to achieve a sufficient wavelength shift. We can clearly see that the wavelength maps for both devices were divided into several areas (numbered 1–7), where each area corresponds to a different SSG-mode. For the active-DBR laser, all areas separated by the boundaries had an almost uniform shape, as shown in Fig. 8(b). This indicates that the lasing oscillations for all SSG-modes were stable, although relatively large tuning

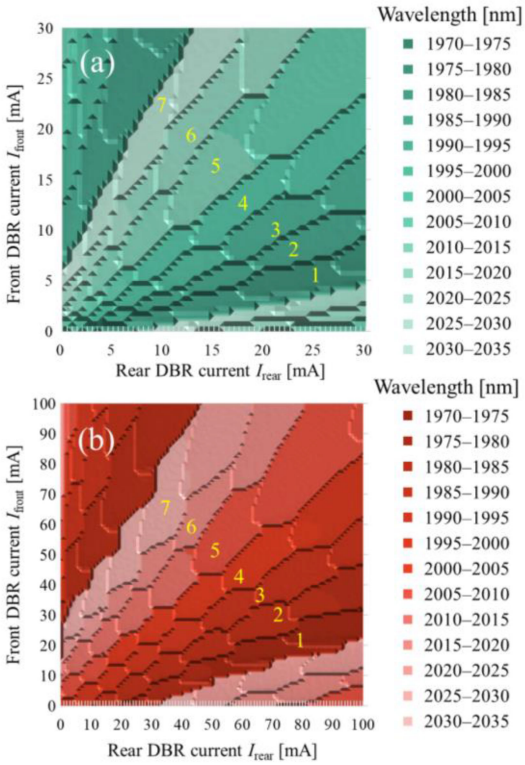

Fig. 8. Contour plot of lasing wavelength of (a) conventional SSG-DBR laser and (b) active DBR type laser.

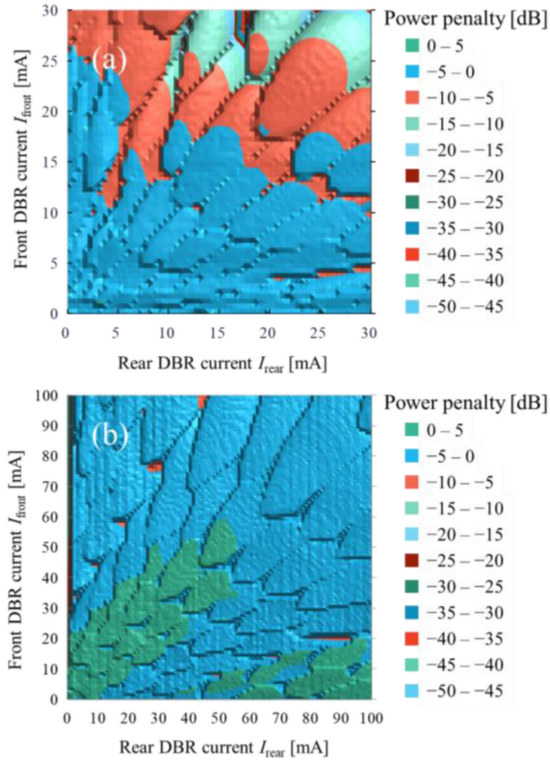

Fig. 9. Contour plot of light intensity for (a) conventional SSG-DBR laser and (b) active DBR type laser.

currents were required to select the SSG-mode. In addition, the active-DBR laser attained almost the same tuning range as the conventional laser, without any gaps.

Fig. 9(a) and (b) shows contour plots of the normalized light intensity for the conventional and active-DBR lasers, respectively. The light intensities were normalized based on the intensity under the condition of 0 mA for both front and rear DBR currents. As shown in Fig. 9(a), the light intensities for the conventional device drastically decreased as the DBR currents increased. In contrast, the intensities of the active-DBR laser shown in Fig. 9(b) were almost at the uniform level, and the reduction of light intensities was less than 5 dB for almost all currents conditions, especially for both the I_{front} and I_{rear} of 100 mA. These findings demonstrate that the decrease of light intensity was dramatically suppressed by the optical gain of the SQW in the active DBR structure.

IV. Quasi-Continuous Tuning Characteristics

Finally, we investigated a quasi-continuous wavelength tuning of the fabricated active-DBR laser and conventional SSG-DBR laser. For the active-DBR laser, we measured the lasing characteristics of 39 wavelength channels consecutively lined up with 100-GHz spacings across the whole tuning range. We first estimated the required currents of I_{front} and I_{rear} for 39 channels from the measured wavelength map shown in Fig. 8(b). In the measurement, the lasing wavelength for each channel was roughly tuned by controlling I_{front} and I_{rear} on the basis of the estimated values. The I_{PC} was also controlled to finely tune the

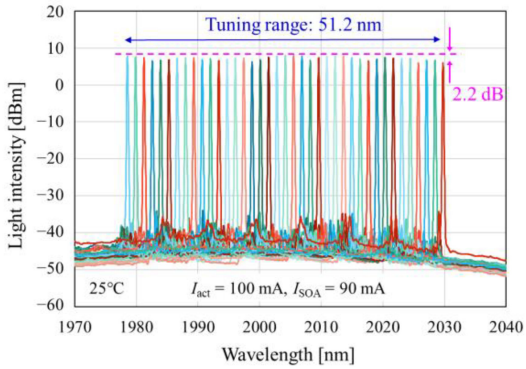

Fig. 10. Superimposed lasing spectra for 39 consecutive channels with 100-GHz spacing.

lasing wavelength and to maximize the side-mode suppression ratio (SMSR) for each channel. For all channels, the active region and the SOA were constantly driven and were not controlled for the light intensity leveling. The I_{act} and I_{SOA} were set to 100 and 90 mA, respectively. The superimposed lasing spectra of the active-DBR laser for all 39 consecutive channels are shown in Fig. 10. As we can see, the lasing wavelengths were accurately tuned from 1978.6 nm for the first channel to 2029.8 nm for the 39$^{\mathrm{th}}$ channel. The lasing characteristics of consecutive wavelength channels were also measured for the conventional SSG-DBR laser. The measured lasing characteristics for all channels are summarized in Fig. 11 for the conventional device and in Fig 12 for the active-DBR laser. For the conventional SSG-DBR laser, the quasi-continuous tuning range of 52 nm

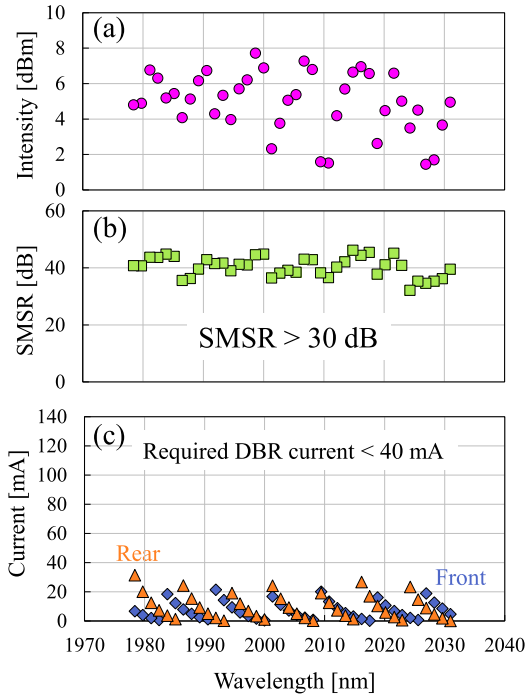

Fig. 11. (a) Light intensities, (b) SMSRs, and (c) required currents for front and rear DBR regions for conventional SSG-DBR laser.

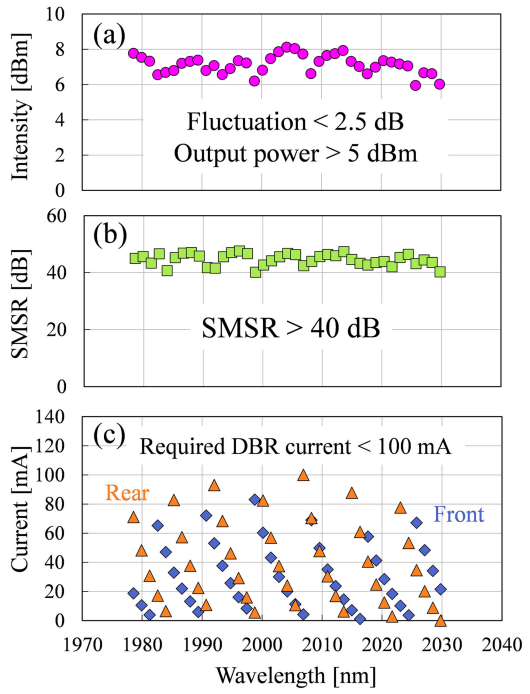

Fig. 12. (a) Light intensities, (b) SMSRs, and (c) required currents for front and rear DBR regions for SSG-DBR laser with active DBR structure.

was achieved, and the maximum light intensity was about 8 dBm. However, the fluctuation of light intensity was as large as about 6.3 dB between each channel. As for the active-DBR laser, it achieved the quasi-continuous tuning range of about 51.2 nm, which is almost the same level as that of the conventional one. The fluctuation of light intensity was suppressed to about 2.2 dB thanks to the optical loss compensation of the SQW inserted in the active DBR structure. In addition to the small fluctuation of light intensity, a high output power of over 5 dBm was achieved for all 39 channels (Fig. 12(a)). As plotted in Fig. 12(b), SMSRs of over 40 dB were achieved for all channels, which is an improvement compared to those of the conventional device thanks to the increase in reflectivity of the DBR section due to the optical loss compensation of the SQW. Fig. 12(c) shows the required currents for I_{front} and I_{rear} for 39 channels. For all channels, the required currents were less than 100 mA for each DBR region. Although relatively large currents were required for the wavelength tuning compared to those for the conventional device, wide wavelength tuning with sufficient lasing characteristics across the whole tuning range was successfully demonstrated for the SSG-DBR laser with the active DBR structure.

V. Conclusion

In this paper, we demonstrated an active-DBR laser with the small fluctuation of light intensity of less than 2.5 dB across a whole tuning range of over 50 nm. To suppress the carrier-induced optical loss during wavelength tuning, a strained InGaAs SQW was inserted into the lattice-matched InGaAs bulk core layer in the DBR sections. The measured wavelength shift due to carrier plasma effect for the single reflection peak of SSGs was more than 8 nm when the front and rear DBR sections were connected and simultaneously swept from 0 to 200 mA. Under this condition, the reduction of light intensity was about 2.7 dB, which is a significant suppression compared to that of the conventional device. Measurements of the lasing wavelength and light intensities for various combinations of front and rear DBR currents showed that all seven SSG-modes could be selectively used for wavelength tuning, and were stably oscillated. The reduction of light intensity was less than 5 dB for almost all conditions, even when the front and rear DBR currents were individually changed from 0 to 100 mA. Finally, the lasing characteristics of 39 consecutive channels with 100-GHz spacings were evaluated to investigate the quasi-continuous tuning. The lasing wavelength was accurately tuned from 1978.6 nm for the first channel to 2029.8 nm for the 39th channel. The fluctuation of intensities was less than 2.2 dB across the whole tuning range of 51.2 nm. Superior lasing operation with high output power (over 5 dBm) and high SMSRs (over 40 dB) was attained for all 39 channels. These results demonstrate that the intensity fluctuation during wavelength tuning can be significantly suppressed and that stable lasing properties can be achieved across the whole tuning range thanks to the optical loss compensation effect of the SQW in the active DBR structure.

References

[1] S. Stephan *et al.*, "Novel InP- and GaSb-based light sources for the near to far infrared," *Semicond. Sci. Technol.*, vol. 31, no. 11, Oct. 2016, Art. no. 113005.

[2] T. Milde *et al.*, "Single mode GaSb diode lasers for sensor applications in a long wavelength regime," *Appl. Opt.*, vol. 56, no. 31, pp. H45–H50, Nov. 2017.

[3] A. Vizbaras *et al.*, "GaSb swept-wavelength lasers for biomedical sensing applications," *IEEE J. Sel. Topics Quantum Electron.*, vol. 25, no. 6, Nov./Dec. 2019, Art. no. 1501812.

[4] M. Hoppe *et al.*, "GaSb-based digital distributed feedback filter laser diodes for gas sensing applications in the mid-infrared region," *J. Opt. Soc. Amer. B*, vol. 38, no. 8, pp. B1–B8, Aug. 2021.

[5] S. Forouhar, A. Ksendzov, A. Larsson, and H. Temkin, "InGaAs/InGaAsP/InP strained-layer quantum well lasers at approximately 2 μm," *Electron. Lett.*, vol. 28, pp. 1431–1432, 1992.

[6] M. Ochiai, H. Temkin, S. Forouher, and R. A. Logan, "InGaAs-InGaAsP buried heterostructure lasers operating at 2.0 μm," *IEEE Photon. Technol. Lett.*, vol. 7, no. 8, pp. 825–827, Aug. 1995.

[7] J. Dong, A. Ubukata, and K. Matsumoto, "Characteristics dependence on confinement structure and single-mode operation in 2-μm compressively strained InGaAs-InGaAsP quantum-well lasers," *IEEE Photon. Technol. Lett.*, vol. 10, no. 4, pp. 513–515, Apr. 1998.

[8] M. Mitsuhara, M. Ogasawara, M. Oishi, H. Sugiura, and K. Kasaya, "2.05-μm Wavelength InGaAs-InGaAs Distributed-feedback multiquantum-well lasers with 10-mW output power," *IEEE Photon. Technol. Lett.*, vol. 11, no. 1, pp. 33–35, Jan. 1999.

[9] R. Phelan, J. O'Carroll, D. Byrne, C. Herbert, J. Somers, and B. Kelly, "$In_{0.75}Ga_{0.25}As$/InP multiple quantum-well discrete-mode laser diode emitting at 2 μm," *IEEE Photon. Technol. Lett.*, vol. 24, no. 8, pp. 652–654, Apr. 2012.

[10] S. Latkowski *et al.*, "Monolithically integrated widely tunable laser source operating at 2 μm," *Optica*, vol. 3, no. 12, pp. 1412–1417, Nov. 2016.

[11] Y. Tohmori, Y. Suematsu, Y. Tushima, and S. Arai, "Wavelength tuning of GaInAsP/InP integrated laser with butt-jointed built-in distributed Bragg reflector," *Electron. Lett.*, vol. 19, no. 17, pp. 656–657, Aug. 1983.

[12] S. Murata, I. Mito, and K. Kobayashi, "Tuning range for 1.5 μm wavelength tunable DBR lasers," *Electron. Lett.*, vol. 24, no. 10, pp. 577–579, May 1988.

[13] N. Fujiwara *et al.*, "Inherently mode-hop-free distributed bragg reflector (DBR) laser array," *IEEE J. Sel. Topics Quantum Electron.*, vol. 9, no. 5, pp. 1132–1137, Sep./Oct. 2003.

[14] B. R. Bennett, R. A. Soref, and J. A. Del Alamo, "Carrier-induced change in refractive index of InP, GaAs and InGaAsP," *IEEE J. Quantum Electron.*, vol. 26, no. 1, pp. 113–122, Jan. 1990.

[15] T. Kanai, N. Fujiwara, Y. Ohiso, H. Ishii, M. Shimokozono, and M. Itoh, "2-μm wavelength tunable distributed Bragg reflector laser," *IEICE Electron. Exp.*, vol. 13, no. 16, Aug. 2016, Art. no. 20160655.

[16] M. Abe *et al.*, "4-nm continuous rapid sweeping spectroscopy in 2-μm band using distributed Bragg reflector laser," *Appl. Phys. B*, vol. 123, no. 10, pp. 1–8, Oct. 2017.

[17] H. Ishii, Y. Tohmori, T. Tamamura, and Y. Yoshikuni, "Super-structure-grating (SSG) for broadly tunable DBR lasers," *IEEE Photon. Technol. Lett.*, vol. 5, no. 4, pp. 393–395, Apr. 1993.

[18] Y. Tohmori, Y. Yoshikuni, T. Tamamura, H. Ishii, Y. Kondo, and M. Yamamoto, "Broad-range wavelength-tunable superstructure grating (SSG) DBR lasers," *IEEE J. Quantum Electron.*, vol. 29, no. 6, pp. 1817–1823, Jun. 1993.

[19] H. Ishii, Y. Tohmori, Y. Yoshikuni, T. Tamamura, and Y. Kondo, "Multiple-phase shift super structure grating DBR lasers for broad wavelength tuning," *IEEE Photon. Technol. Lett.*, vol. 5, no. 6, pp. 613–615, Jun. 1993.

[20] H. Ishii, H. Tanobe, F. Kanso, Y. Tohmori, Y. Kondo, and Y. Yoshikuni, "Quasicontinuous wavelength tuning in super-structure-grating (SSG) DBR lasers," *IEEE J. Quantum Electron.*, vol. 32, no. 3, pp. 433–441, Mar. 1996.

[21] T. Shindo, N. Fujiwara, Y. Ohiso, T. Sato, and H. Matsuzaki, "Quasi-continuous tuning of a 1.3-μm-wavelength superstructure grating distributed Bragg reflector laser by enhancing carrier-induced refractive index change," *Opt. Exp.*, vol. 29, no. 1, pp. 232–243, Jan. 2021.

[22] V. Jayaraman, Z.- M. Chuang, and L. A. Coldren, "Theory, design, and performance of extended tuning range semiconductor lasers with sampled gratings," *IEEE J. Quantum Electron.*, vol. 29, no. 6, pp. 1824–1834, Jun. 1993.

[23] M. Oberg, S. Nilsson, K. Streubel, J. Wallin, L. Backbom, and T. Klinga, "74 nm wavelength tuning range of an InGaAsP/InP vertical grating assisted codirectional coupler laser with rear sampled grating reflector," *IEEE Photon. Technol. Lett.*, vol. 5, no. 7, pp. 735–737, Jul. 1993.

[24] T. Shindo *et al.*, "2.0-μm wavelength superstructure-grating-(SSG-) distributed Bragg reflector laser with tuning range of over 50 nm," *IEEE Photon. Technol. Lett.*, vol. 33, no. 13, pp. 641–644, Jul. 2021.

[25] N. Fujiwara *et al.*, "Single-mode 140 nm swept light source realized by using SSG-DBR lasers," *Proc. SPIE*, vol. 6847, 2008, Art. no. 684713.

[26] N. Fujiwara *et al.*, "140-nm quasi-continuous fast sweep using SSG-DBR lasers," *IEEE Photon. Technol. Lett.*, vol. 20, no. 12, pp. 1015–1017, Jun. 2008.

[27] Y. A. Akulova *et al.*, "Widely tunable electroabsorption-modulated sampled-grating DBR laser transmitter," *IEEE J. Sel. Topics Quantum Electron.*, vol. 8, no. 6, pp. 1349–1357, Nov./Dec. 2002.

[28] A. J. Ward *et al.*, "Monolithic integration of AlInGaAs DS-DBR tunable laser and AlInGaAs MZ modulator with small footprint, low power dissipation and long-haul 10Gb/s performance," in *Proc. 39th Eur. Conf. Exhib. Opt. Commun.*, 2013, pp. 1–3.

[29] Y. Ueda *et al.*, "2-μm band active distributed Bragg reflector laser for CO_2 gas sensing," *Appl. Phys. Exp.*, vol. 12, no. 9, Aug. 2019, Art. no. 092011.

[30] H. Arimoto *et al.*, "A wavelength-tunable short-cavity DBR laser with active distributed Bragg reflector," *IEICE Electron. Exp.*, vol. 2, no. 5, pp. 170–175, Feb. 2005.

[31] H. Arimoto *et al.*, "Wavelength-tunable short-cavity DBR laser array with active distributed Bragg reflector," *J. Lightw. Technol.*, vol. 24, no. 11, pp. 4366–4371, Nov. 2006.

[32] T. Shindo *et al.*, "2-μm wavelength superstructure grating active DBR laser with $<$ 2.5-dB fluctuation of light intensity across whole tuning range of over 50 nm," in *Proc. 27th Int. Semicond. Laser Conf.*, 2021, pp. 1–2.